



**HAL**  
open science

# Design insights for upscaling spontaneous microfluidic emulsification devices based on behavior of the Upscaled Partitioned EDGE device

Sten ten Klooster, Claire Berton-Carabin, Karin Schroën

## ► To cite this version:

Sten ten Klooster, Claire Berton-Carabin, Karin Schroën. Design insights for upscaling spontaneous microfluidic emulsification devices based on behavior of the Upscaled Partitioned EDGE device. Food Research International, 2023, 164, pp.112365. 10.1016/j.foodres.2022.112365 . hal-04026065

**HAL Id: hal-04026065**

**<https://hal.inrae.fr/hal-04026065>**

Submitted on 13 Mar 2023

**HAL** is a multi-disciplinary open access archive for the deposit and dissemination of scientific research documents, whether they are published or not. The documents may come from teaching and research institutions in France or abroad, or from public or private research centers.

L'archive ouverte pluridisciplinaire **HAL**, est destinée au dépôt et à la diffusion de documents scientifiques de niveau recherche, publiés ou non, émanant des établissements d'enseignement et de recherche français ou étrangers, des laboratoires publics ou privés.



Distributed under a Creative Commons Attribution 4.0 International License



# Design insights for upscaling spontaneous microfluidic emulsification devices based on behavior of the Upscaled Partitioned EDGE device

Sten ten Klooster<sup>a,\*</sup>, Claire Berton-Carabin<sup>a,b</sup>, Karin Schroën<sup>a</sup>

<sup>a</sup> Laboratory of Food Process Engineering, Wageningen University, P.O. Box 17, Bornse Weilanden, 9, 6708 WG Wageningen, the Netherlands

<sup>b</sup> INRAE, BIA, 44000 Nantes, France

## ARTICLE INFO

### Keywords:

Microfluidics  
Emulsion  
Monodisperse  
Droplet  
Food  
Emulsifier  
Interface

## ABSTRACT

Microfluidic emulsification has the potential to produce emulsions with very controlled droplet sizes in a subtle manner. To support in unleashing this potential, we provide guidelines regarding upscaling based on the performance of Upscale Partitioned EDGE (UPE) devices, using rapeseed oil as the to-be-dispersed phase and whey proteins as the emulsifier. The UPE<sub>5x1</sub> device (11,000 droplet formation units (DFUs) of  $5 \times 1 \mu\text{m}$ ) produced 3.5- $\mu\text{m}$  droplets (CV 3.2 %) at 0.3 mL/h; UPE<sub>10x2</sub> (8,000 DFUs of  $10 \times 2 \mu\text{m}$ ) produced 7- $\mu\text{m}$  droplets (CV 3.2 %) at 0.5 mL/h, and at higher pressures, 32- $\mu\text{m}$  droplets (CV 3–4 %) at 4 mL/h. These productivities are relatively high compared to those of other devices reported in literature (e.g., Microchannel, Tsukuba and Millipede, Harvard).

Based on these results, and on others from literature, we conclude that: (1) the continuous phase channel dimensions need to be chosen such that they allow for gradual filling of this channel with droplets without decreasing the pressure over the droplet formation units significantly; (2) the dispersed phase supply channel design should create a wide stable droplet formation pressure range to increase productivity; and (3) higher productivities can be obtained through the choice of the ingredients used; low viscosity dispersed phase and an emulsifier that increases the interfacial tension without negatively affecting device wettability is preferred (e.g., whey protein outperforms Tween 20). These results and design guidelines are expected to contribute to the first food emulsion products prepared with microfluidics.

## 1. Introduction

Microfluidic emulsification is an emerging technique to produce, amongst others, food and pharma emulsions with a highly controlled droplet size in a very subtle manner (Schroen, Bliznyuk, Muijlwijk, Sahin, & Berton-Carabin, 2015; Zhu & Wang, 2017). It is also an excellent tool to perform high throughput experiments in the fields of biology and chemistry compared to conventional approaches (Neves, Wang, Kobayashi, & Nakajima, 2017; Shang, Cheng, & Zhao, 2017; Teh, Lin, Hung, & Lee, 2008). Besides, microfluidic emulsification has also been widely used in food science as analytical tools to study e.g. lipid oxidation (Neves et al., 2017), emulsion physical stability (Hinderink et al., 2021; Krebs, Schroën, & Boom, 2012; Muijlwijk et al., 2017), and so on, as recently reviewed (Schroen et al., 2021).

In microfluidic emulsification devices, a dispersed phase is contacted with a continuous phase in a controlled manner by making use of very small channels (van Dijke, de Rooter, Schroën, & Boom, 2010). As a result, a droplet is formed either spontaneously or due to the shear

exerted by the continuous phase flow. The disadvantage of microfluidic devices that operate by such shear forces (e.g., T- and Y-junctions, flow-focussing and co-flow devices) is that the flow of both phases has to be controlled very precisely to make monodisperse droplets, which complicates tuning droplet size and reaching a specific concentration of oil in the final emulsion (Vladisavljević, Kobayashi, & Nakajima, 2012; Zhu & Wang, 2017). Spontaneous microfluidic emulsification devices are more practical for scale-up because droplet formation occurs through a change in Laplace pressure of the dispersed phase, which is also the only phase that needs to be controlled precisely (Kawakatsu, Kikuchi, & Nakajima, 1997; Schroën, Bliznyuk, Muijlwijk, Sahin, & Berton-Carabin, 2015).

In literature, several upscaled spontaneous microfluidic emulsification devices can be found, all with a specific device geometry. It is difficult to compare these devices because different assessment criteria exist: droplet size (often smaller droplets are desired), droplet mono-dispersity (often assessed by the coefficient of variation (CV)), droplet formation frequency per active droplet formation unit (DFU), fraction of

\* Corresponding author.

E-mail addresses: [sten.tenklooster@wur.nl](mailto:sten.tenklooster@wur.nl) (S. ten Klooster), [claire.ber-ton-carabin@inrae.fr](mailto:claire.ber-ton-carabin@inrae.fr) (C. Berton-Carabin), [karin.schroen@wur.nl](mailto:karin.schroen@wur.nl) (K. Schroën).

<https://doi.org/10.1016/j.foodres.2022.112365>

Received 20 August 2022; Received in revised form 9 December 2022; Accepted 24 December 2022

Available online 28 December 2022

0963-9969/© 2022 The Authors. Published by Elsevier Ltd. This is an open access article under the CC BY license (<http://creativecommons.org/licenses/by/4.0/>).

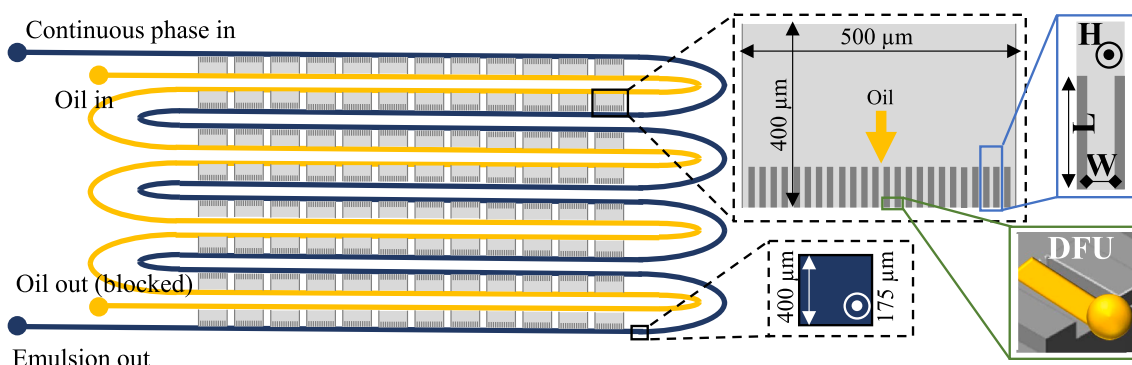


**Fig. 1.** Top-view design of the Upscaled Partitioned EDGE chips used in this research. The blue ‘twisted road’ channel is the continuous phase channel, and the yellow ‘twisted road’ channel is the to-be-dispersed phase channel. The gray rectangular areas in between these channels are the main plateaus that contain the micro-plateaus with the Droplet Formation Units (DFU). A 3D representation of a DFU is shown in the right lower corner, showing oil – in yellow – being pushed out of the DFU and forming a droplet ready to detach. Dimensions of the DFUs are in Table 1. This illustration is not to scale; only 12 out of the 42 main plateaus are shown per row.

**Table 1**

Characteristic dimensions of the Upscaled Partitioned EDGE (UPE) devices.

Coding used	Dimensions of micro-plateaus [ $L \cdot W \cdot H$ ] [ $\mu\text{m}$ ]	Number of main plateaus [-]	Number of micro-plateaus per main plateau [-]	Total number of micro-plateaus (DFUs) [-]
UPE <sub>5 x 1</sub>	40 · 5 · 1	336	33	11,088
UPE <sub>10 x</sub>	40 · 10 · 2	336	24	8,064

active DFUs, productivity per unit area ( $\text{L}/\text{m}^2\text{h}$ ), or the actual oil throughput; additionally, throughputs per DFU are higher when producing larger droplets (Stolovicki, Ziblat, & Weitz, 2018). The intrinsic properties of the components used also influence productivity: for example, the higher the continuous and dispersed phase viscosities, the lower the productivity (Kobayashi, Murayama, Kuroiwa, Uemura, & Nakajima, 2009; van Dijke, Kobayashi, et al., 2010; Vladislavjević, Kobayashi, & Nakajima, 2011). In addition, a higher oil–water interfacial tension usually leads to a higher productivity (Kobayashi, Mukata, & Nakajima, 2005c). This (dynamic) oil–water interfacial tension is also affected by the emulsifier type and concentration. Besides, the emulsifier can change the wetting of the channel walls, which may lead to a higher productivity (Sahin, Bliznyuk, Cordova, & Schroën, 2016). The differences in assessment criteria and in experimental set-ups make it rather difficult to compare studies fairly.

In the current research, we focus on droplets that are below  $10 \mu\text{m}$ , and thus relevant for food applications; it would be even more favourable from the point of product physical stability if we could produce droplets that are smaller than  $5 \mu\text{m}$  and for some products even below  $1 \mu\text{m}$  (Gijbetsen-Abrahamse, van der Padt, & Boom, 2004; Leal-Calderon, Schmitt, & Bibette, 2007). Devices capable of producing droplets  $< 5 \mu\text{m}$  have been reported, but the productivities were very low ( $10^{-3} \text{ mL oil per h}$ ), which limits the options for characterizing the obtained emulsion (Kobayashi et al., 2001; Kobayashi, Uemura, & Nakajima, 2007). Here, we present a device called Upscaled Partitioned EDGE (UPE), which can be flexibly deployed to make different droplet sizes and oil volume fractions, starting from different emulsifiers: Tween 20 and whey proteins as prominent representatives of food-grade surfactant and protein emulsifiers, respectively. We use several assessment criteria, such as droplet sizes, true oil droplet production ( $\text{mL}/\text{h}$ ) and productivity per chip area ( $\text{L}/\text{m}^2\text{h}$ ) that are normalized where possible (e.g., for dispersed phase viscosity (van Dijke, Kobayashi, et al., 2010)) to compare our device with other upscaled devices in literature. Finally, we provide guidelines for the design and operation of upscaled microfluidic emulsification devices.

## 2. Materials and methods

### 2.1. Materials

Rapeseed oil was kindly provided by Unilever (Wageningen, the Netherlands) and stripped with alumina powder (MP EcoChromet ALUMINA N, Activity: Super I, Biomedicals) to remove surface-active impurities and endogenous antioxidants (Berton, Genot, & Ropers, 2011). Whey protein isolate (WPI, purity 97.0–98.4 % (BiPro®, Davisco, Switzerland) and Tween 20 (Sigma-Aldrich, Zwijndrecht, the Netherlands) were used as emulsifiers. Sodium phosphate monobasic dihydrate and sodium phosphate dibasic dihydrate (Sigma-Aldrich, Zwijndrecht, the Netherlands) were used to make the phosphate buffer (pH 7.0). For cleaning the chips, we used ethanol, purity 96 % v/v (VWR International B.V., Amsterdam, the Netherlands) and piranha solution, which is a 3:1 v/v ratio of sulphuric acid, purity 96 % (Sigma-Aldrich, Zwijndrecht, the Netherlands) and 35 wt% hydrogen peroxide (Sigma-Aldrich, Zwijndrecht, the Netherlands). Assay reagent for measuring the triglyceride (TAG) content and a standard containing TAGs (Triglycerides liquicolor mono kit) were purchased from HUMAN (HUMAN Gesellschaft für Biochemica und Diagnostica mbH, Wiesbaden, Germany). Ultrapure water ( $18.2 \text{ M}\Omega$ ) was used for all experiments and prepared using a Milli-Q system (Millipore Corporation, Billerica, MA, USA).

### 2.2. Chip design

The Upscaled Partitioned EDGE (Edge-based droplet generation) (UPE) microfluidic chips were designed in our lab and produced in glass by deep reactive ion etching (DRIE) (Micronit Microfluidics, Enschede, The Netherlands). The relatively deep continuous and dispersed phase channels and the shallow plateaus, including the micro-plateaus (droplet formation units: DFUs), were etched into two separate glass substrates, which were later bonded together and diced. In the relatively long and deep continuous phase channel, the droplets were formed and collected. The layout of the microchips is shown in Fig. 1; the dimensions of the micro-plateaus are specified in Table 1.

### 2.3. Continuous and dispersed phase preparation

The day before emulsion production with the microfluidic chips, the emulsifier (either 5.0 wt% WPI or 2 wt% Tween 20) was dissolved in 10 mM phosphate buffer (pH = 7.0) and gently stirred overnight at  $4 \text{ }^\circ\text{C}$ . Prior to use, the dispersed and continuous phase liquids were filtered using a  $0.22\text{-}\mu\text{m}$  filter (Minisart High-Flow, Sartorius Stedim Biotech GmbH, Goettingen, Germany).

## 2.4. Chip cleaning

The cleaning of the chips is one of the most critical points in microfluidic emulsification; if the chip is not properly cleaned, the productivity can be reduced (Zhang, Kobayashi, Neves, Uemura, & Nakajima, 2015). After each experiment was completed, the chips (including the plateaus) were flushed with ethanol, sonicated in ethanol for 90 min and then in water for 10 min. Next, the chip was baked in an oven at 500 °C for 2 h. The chip was stored until the day before the experiment. The day before the experiment, the chip was sonicated (Branson 1800, Brookfield, CT, USA) in a glass beaker with piranha (1:3 v/v mixture of sulphuric acid and 35 % hydrogen peroxide) for 90 min followed by 90 min sonication in ultrapure water, and it was left in ultrapure water overnight. On the day of the experiment, the chip was rinsed with ultrapure water to remove any leftovers of cleaning chemicals from the channels.

## 2.5. Chip operation

Once cleaned, the device may be used. The microfluidic chip was placed in a chip holder from Micronit (Fluidic Connect PRO Chip Holder with 4515 Inserts, Micronit Microfluidics, Enschede, The Netherlands). After the main channels were wetted with the continuous phase by flowing this phase into the chip gently, the oil was pushed into the dispersed phase channel. When rinsed thoroughly, the dispersed phase outlet was blocked (Fig. 1). Next, the dispersed phase was pressurized across the plateau, through the micro-plateaus and finally through the DFUs. At the DFUs, droplets were formed that were carried away by the cross-flowing continuous phase (Fig. 1). This cross-flow will not influence droplet size since the cross-flow is not needed for droplet formation in these devices (Sahin & Schroën, 2015). The pressures, and thereby the flows, were controlled through a microfluidic control system (Elveflow OB1, MK3, Elveflow®, France), and droplet formation was monitored by using an inverted microscope (Axiovert 200 MAT, Carl Zeiss B.V., The Netherlands), which was connected to a high-speed camera (FASTCAM SA-Z, Photron Limited, Japan). The maximum frame rate was 100,000 frames per s, and the resolution was 0.973 or 0.402 μm/pixel.

## 2.6. Productivity

The maximum emulsion productivity was measured by determining droplet size in combination with the droplet formation frequencies and by the actual oil content (approximately 5 wt%) of the collected emulsions. Both methods are described below.

### 2.6.1. Droplet sizes and frequencies

The productivity was determined by multiplying the average droplet volume (see section 2.7) with the average droplet formation frequency per DFU and with the amount of DFUs per chip (Table 1). The average droplet formation frequency was determined by using a custom-written script in image analysis software (Matlab R2019B) on high-speed recordings during production. The recordings were taken at several locations on the chip and at several time points during production to ensure representative data.

### 2.6.2. Triglyceride content of collected emulsions

In addition, the productivity was determined by weighing the amount of emulsion collected over time, and measuring the oil content using a colorimetric method to determine the triglyceride (TAG) content (Triglycerides Liquicolor Mono kit, HUMAN) (Jacobs & Vandenmark, 1960; Trinder, 1969). In brief, the samples were diluted to a range of 0.5–4 g/L. Next, the droplets were broken up in smaller droplets by sonication with the Branson Sonifier SFX550 (Brookfield, CT, USA) equipped with a sonication tip 1/8' tapered microtip (Branson, Brookfield, CT, USA) at an amplitude of 35 % for 15 s. This was done because a large amount of oil–water interface was required to hydrolyse the

triglycerides and thereby obtain accurate results using this assay kit. The droplet size distribution of the broken droplets was independent of the initial droplet size (Fig. A1). Next, about 20 μL of sample were weighed into a 2-mL microtube, and 1 mL of assay reagent was added. The assay reagent content was: 50 mmol/L PIPES buffer (pH 7.5), 5 mmol/L 4-chlorophenol, 0.25 mmol/L 4-aminoantipyrine, 4.5 mmol/L magnesium ions, 2 mmol/L ATP, 1.3 U/mL lipases, 0.5 U/mL peroxidase, 0.4 U/mL glycerol kinase, and 1.5 U/mL glycerol-3-phosphate oxidase. The samples were incubated in a heating block at 800 rpm for 20 min at 20 °C. Next, the absorbance was measured at a wavelength of 500 nm. A calibration curve was generated with TAG dispersions with known concentrations ranging from 0.5 to 4 g/L. Finally, the productivity was calculated based on the amount of collected sample and its TAG content.

## 2.7. Droplet sizes measurements

### 2.7.1. Image analysis

A small volume (3 μL) of sample was taken from the collected emulsions and analysed using a Carl Zeiss AxioScope A1 optical microscope (Carl Zeiss BV, Breda, the Netherlands) equipped with a camera (AxioCam Mrc5). At least 75 droplets per data point were analysed using a custom-written script in image analysis software (Matlab R2019b) to determine the average droplet size, which is sufficient when droplets are very monodisperse (Deng, Schroën, & de Ruiter, 2021). With this script, the droplet diameter is calculated from the circumference of the droplet. Since the droplet volume scales with the droplet diameter to the power of three, a small systematic error leads to a large error in productivity (section 2.6); therefore, as a check, the centre-to-centre distance of clustered droplets was determined, and with that a correction factor could be calculated (Table A1). The productivities determined by the different methods described above (section 2.6.1 and 2.6.2) were in line with each other (Fig. A2); therefore, confirming the appropriateness of the methods used.

### 2.7.2. Statistics droplet sizes

The size distribution of the droplets was expressed as a coefficient of variation (CV), which was defined as:

$$CV = \frac{\sigma}{d_{dr}} \cdot 100 \quad (1)$$

where  $\sigma$  is the standard deviation of the droplet diameters, and  $d_{dr}$  is the number-average droplet diameter. Based on previous research, droplets with a CV below 10 % can be considered monodisperse (van Dijke, Veldhuis, Schroën, & Boom, 2009).

## 2.8. Viscosity

The viscosity of the rapeseed oil used was measured at 22 °C (the lab temperature) with a rheometer (Anton Paar Physica MCR 301, Anton Paar, Oosterhout, the Netherlands) at a shear rate of 100 s<sup>-1</sup>.

## 2.9. Calculations

The pressure difference ( $\Delta P$ ) working over the DFUs is calculated as the applied pressure over the dispersed phase minus the applied pressure over the continuous phase.

The flow resistances ( $R$ ) of the devices can be calculated with a Hagen-Poiseuille-based equation for a rectangular channel:

$$R = \frac{12\eta l}{1 - 0.63(\frac{h}{w})} \frac{1}{h^3 w} \quad (2)$$

where  $\eta$  is the viscosity,  $l$  the length,  $h$  the height and  $w$  the width of the channel, respectively. Equation (2) was used to calculate the flow resistance of a micro-plateau (actual DFU) and the main plateau separately. The total flow resistance of main and micro-plateaus ( $R_t$ ) was



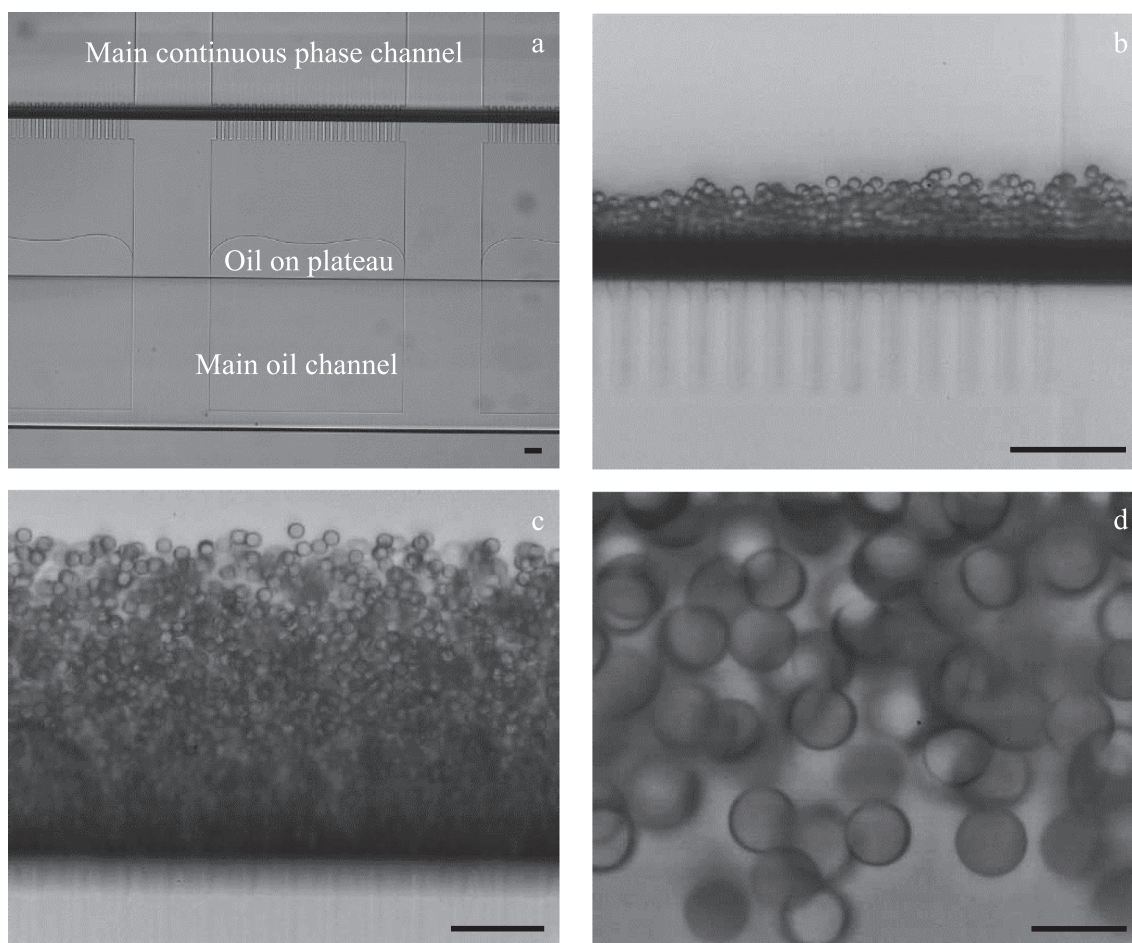


**Fig. 2.** The UPE<sub>10x2</sub> device in operation: (a) start of oil flow over the main plateaus, (b) droplet formation at the first DFUs at low pressure, (c) production of small monodisperse droplets at maximum productivity, (d) production of large monodisperse droplets, using the same chip, at higher dispersed phase pressures. Scale bars represent 50  $\mu\text{m}$ .

defined as:

$$R_t = \frac{R_{mi}}{n_{mi}} + R_{ma} \quad (3)$$

where  $R_{mi}$  is the flow resistance of the micro-plateau,  $n_{mi}$  is the number of micro-plateaus per main plateau and  $R_{ma}$  is the flow resistance of the main plateaus. The flow resistance of the whole shallow connection, expressed per micro-plateau ( $R_{t,mi}$ ), was calculated as:

$$R_{t,mi} = R_t \cdot n_{mi} \quad (4)$$

This flow resistance was then used to calculate the flow ( $\phi$ ) at a certain pressure ( $P$ ):

$$\phi = \frac{P - P_{LP}}{R_{t,mi}} \quad (5)$$

The Laplace pressure ( $P_{LP}$ ) of a bare oil–water interface can be calculated by:

$$P_{LP} = \gamma_b \left( \frac{1}{r_1} + \frac{1}{r_2} \right) \quad (6)$$

where  $\gamma_b$  is the interfacial tension of the bare oil–water interface,  $r_1$  and  $r_2$  the radii of curvature of the meniscus inside the micro-plateau, in this case, half the width and half the height (of the DFUs).

### 3. Results and discussion

In Sections 3.1 and 3.2, the performance of the Upscaled Partitioned

EDGE (UPE) device is discussed and in Section 3.3, UPE is compared with other upscaled devices from literature. Section 3.4 provides guidelines for upscaling spontaneous microfluidic emulsification devices.

#### 3.1. Operation of UPE

The chips, with 8,000–11,000 DFUs (Table 1), were operated by first pushing the continuous phase in the respective channel, after which the applied pressure over the dispersed phase was increased until the oil flows over the shallow plateaus at the so-called breakthrough pressure (Fig. 2a), which equals the Laplace pressure of the oil–water meniscus that works in the opposite direction (van Dijke, Veldhuis, Schroën, & Boom, 2010). Upon further increasing the pressure, droplet formation started and the droplet formation frequency increased with pressure, whereas the droplet size was barely affected (Fig. 2bc) (Sahin & Schroën, 2015). When the pressure was further increased, the so-called blow-up pressure was reached, above which larger monodisperse droplets were formed through a physical push by neighboring droplets in a cascaded fashion (Fig. 2d) (Ten Klooster, Sahin, & Schroën, 2019).

##### 3.1.1. Different droplet sizes by UPE

We produced small emulsion droplets in the first pressure regime at the maximum productivity with the UPE<sub>5x1</sub> and UPE<sub>10x2</sub> chips, using either 5 wt% WPI or 2 wt% Tween 20 (Figs. 3 and 4, respectively). The droplets were very monodisperse with CVs ranging from 2.7 to 7.8 % (discussed in more detail in section 3.4). The droplets produced with

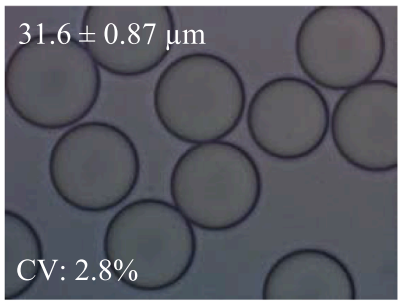
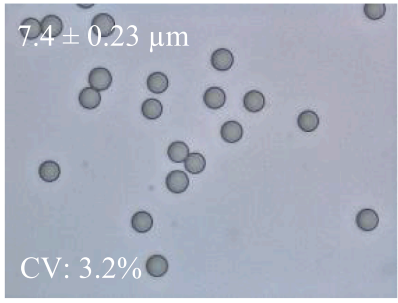
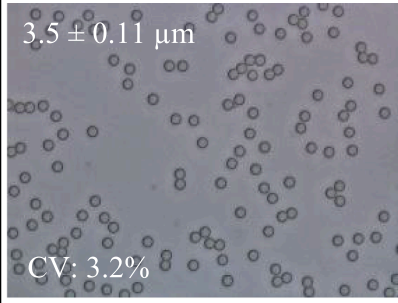
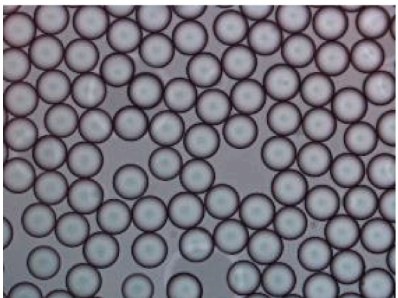
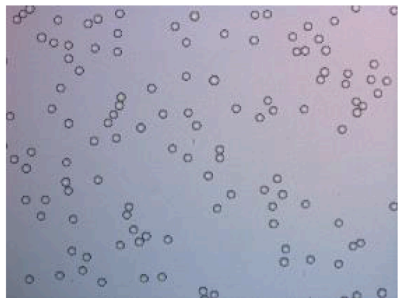
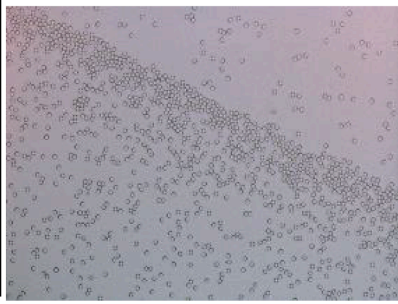
Magnification	Large droplets second regime, UPE <sub>10 x 2</sub>	Intermediate droplets first regime, UPE <sub>10 x 2</sub>	Small droplets first regime, UPE <sub>5 x 1</sub>
100x	 <p>31.6 ± 0.87 μm CV: 2.8%</p>	 <p>7.4 ± 0.23 μm CV: 3.2%</p>	 <p>3.5 ± 0.11 μm CV: 3.2%</p>
40x			

Fig. 3. Light microscopy images of the produced rapeseed oil droplets at the maximum productivity with 5 wt% WPI in the continuous phase.

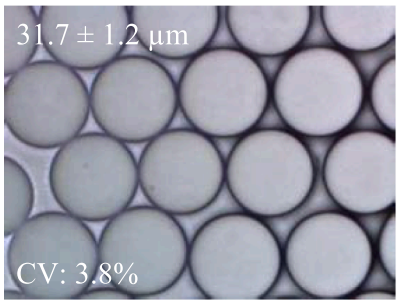
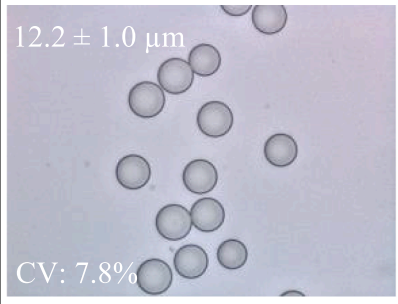
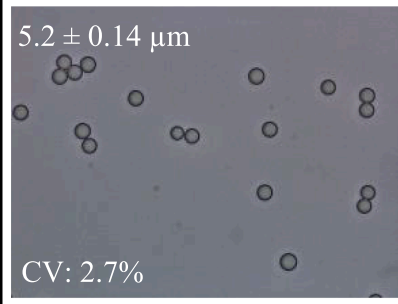
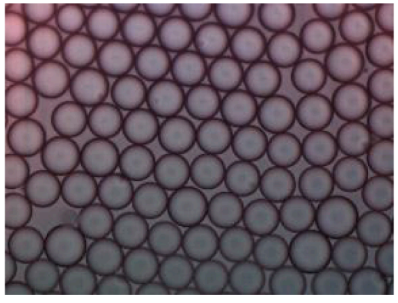
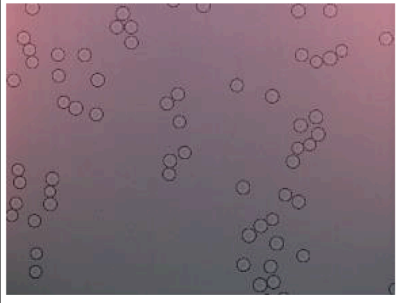
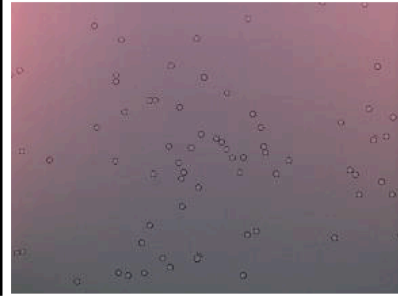
Magnification	Large droplets second regime, UPE <sub>10 x 2</sub>	Intermediate droplets first regime, UPE <sub>10 x 2</sub>	Small droplets first regime, UPE <sub>5 x 1</sub>
100x	 <p>31.7 ± 1.2 μm CV: 3.8%</p>	 <p>12.2 ± 1.0 μm CV: 7.8%</p>	 <p>5.2 ± 0.14 μm CV: 2.7%</p>
40x			

Fig. 4. Light microscopy images of the produced rapeseed oil droplets at the maximum productivity with 2 wt% of Tween 20 in the continuous phase.

**Table 2**

Applied pressures over the different phases for droplet formation at maximum productivities.

Chip	Emulsifier (wt %)	Breakthrough Pressure (mbar)	Dispersed phase pressure (mbar)	Continuous phase pressure (mbar)	Pressure difference $\Delta P$ (mbar)	Theoretical $\Delta P_{LP}$ bare O/W meniscus (mbar)
UPE <sub>5x1</sub>	5 % WPI	350	2,710	150	2,560	720
UPE <sub>5x1</sub>	2 % Tween 20	170	725	25	700	720
UPE <sub>10x2</sub>	5 % WPI	175	920	290	630	360
UPE <sub>10x2</sub>	2 % Tween 20	90	260	60	200	360

**Table 3**

Overview of upscaled spontaneous microfluidic emulsification devices reported in literature that produce droplets < 80  $\mu\text{m}$ . The main focus was on oil-in-water emulsions, but the bottom seven rows are about water-in-oil emulsion generation devices. Abbreviations: (P)EDGE = (partitioned) edge-based droplet generation, WP(D)(C) = whey protein (concentrate) (isolate), H<sub>2</sub>O = distilled water, SDS = sodium dodecyl sulfate, PVA = polyvinylalcohol, (A)ST=(Asymmetric) straight-through, MC = microchannel, PCL = polycaprolactone, PLA = poly(D,L-lactic) acid, DCM = dichloromethane, TGCR = tetraglycerin monolaurate condensed ricinoleic acid esters, PEG = poly(ethylene)glycol, FL = fluorinated, FLo = Fluoro. Distilled or ultrapure water was used for all experiments.

Article	Name device	H · W ( $\mu\text{m}$ )	Dispersed phase	$\eta_d$ (mPa s)	Continuous phase	DFUs
This paper	Upscaled P-EDGE (UPE_5x1)	1 · 5	Stripped rapeseed oil	63.8	H <sub>2</sub> O, 2 % Tween 20	11,088
This paper	Upscaled P-EDGE (UPE_5x1)	1 · 5	Stripped rapeseed oil	63.8	H <sub>2</sub> O, 5 % WPI	11,088
This paper	Upscaled P-EDGE (UPE_10x2)	2 · 10 (low P)	Stripped rapeseed oil	63.8	H <sub>2</sub> O, 2 % Tween 20	8,064
This paper	Upscaled P-EDGE (UPE_10x2)	2 · 10 (low P)	Stripped rapeseed oil	63.8	H <sub>2</sub> O, 5 % WPI	8,064
This paper	Upscaled P-EDGE (UPE_10x2)	2 · 10 (high P)	Stripped rapeseed oil	63.8	H <sub>2</sub> O, 2 % Tween 20	8,064
This paper	Upscaled P-EDGE (UPE_10x2)	2 · 10 (high P)	Stripped rapeseed oil	63.8	H <sub>2</sub> O, 5 % WPI	8,064
(Van Dijke, Schroën, Van der Padt, & Boom, 2010)	EDGE-R	1.2 · 500	Sunflower oil	50	H <sub>2</sub> O, 6 wt% WPC	196
(Van Dijke, Schroën, Van der Padt, & Boom, 2010)	EDGE-R	1.2 · 500	Hexadecane	3.4	H <sub>2</sub> O, 6 wt% WPC	196
(Sahin & Schroën, 2015)	P-EDGE	2 · 5 (low P)	Hexadecane	3.4	H <sub>2</sub> O, 0.5 wt% SDS	33
(Sahin & Schroën, 2015)	P-EDGE	2 · 5 (high P)	Hexadecane	3.4	H <sub>2</sub> O, 0.5 wt% SDS	33
(Ten Klooster et al., 2022)	Multi EDGE	2 · 10	Hexadecane	3.4	H <sub>2</sub> O, 0.5 wt% SDS	75,000
(Ofner et al., 2017)	Step	100 · 20	Hexadecane	3.4	H <sub>2</sub> O, 2 wt% PVA	364
(Kobayashi et al., 2003)	ST-MC	9.6 · 48.7	Refined soybean oil	50.4	H <sub>2</sub> O 1 wt% Tween 20	4,300
(Kobayashi et al., 2003)	ST-MC	9.6 · 48.7	Refined soybean oil	50.4	H <sub>2</sub> O 1 wt% SDS	4,300
(Kobayashi et al., 2005b)	AST-MC	11 · 104	Decane	0.87	H <sub>2</sub> O 1 wt% SDS	10,313
(Kobayashi et al., 2005b)	AST-MC	11 · 104	Refined soybean oil	50.4	H <sub>2</sub> O 1 wt% SDS	10,313
(Kobayashi et al., 2007)	MC	0.32 · 3.2	Refined soybean oil	50.4	H <sub>2</sub> O 1 wt% SDS	1,500
(Kobayashi et al., 2007)	MC	0.72 · 3.2	Refined soybean oil	50.4	H <sub>2</sub> O 1 wt% SDS	1,500
(Kobayashi et al., 2007)	MC	1.4 · 3.2	Refined soybean oil	50.4	H <sub>2</sub> O 1 wt% SDS	1,500
(Kobayashi et al., 2001)	MC (SMC-B4)	1.2 · missing	Refined soybean oil	50.4	H <sub>2</sub> O, 1.5 wt% Tween 80	1,200
(Kobayashi et al., 2005c)	ST-MC	6.6 · 26.7	Refined soybean oil	50.4	H <sub>2</sub> O, 1 wt% SDS	211,248
(Kobayashi et al., 2005c)	ST-MC	6.6 · 26.7	Silicone oil	48	H <sub>2</sub> O, 1 wt% SDS	211,248
(Kobayashi et al., 2010)	MC	2 · 40	Refined soybean oil	50.4	H <sub>2</sub> O, 1 wt% SDS	11,900
(Vladisavljević et al., 2011)	AST-MC	10 · 50	Refined soybean oil	50	H <sub>2</sub> O, 2 % Tween 20	23,348
(Vladisavljević et al., 2011)	AST-MC	10 · 50	Medium chain triglycerides	20	H <sub>2</sub> O, 2 % Tween 20	23,348
(Vladisavljević et al., 2011)	AST-MC	10 · 50	Tetradecane	2.7	H <sub>2</sub> O, 2 % Tween 20	23,348
(Kobayashi, Neves, Wada, Uemura, & Nakajima, 2012)	AST-MC array	17 · 119	Tetradecane	2.7	H <sub>2</sub> O, 2 wt% Tween 20	24,772
(Vladisavljević et al., 2018)	MC (step), DMS6 design 1	5 · 18	2 wt% PCL (1), 1 wt% PLA (2) in DCM (3)	0.4	H <sub>2</sub> O, 2 wt% PVA	540
(Vladisavljević et al., 2018)	MC (step), DMS6 design 2	4 · 8	2 wt% PCL (1), 1 wt% PLA (2) in DCM (3)	0.4	H <sub>2</sub> O, 2 wt% PVA	1,850
(Kobayashi et al., 2008)	ST-MC, MC TMS 11–2	2.3 · 10	Refined Soybean oil	50.4	H <sub>2</sub> O, 1 wt% SDS	23,548
(Kobayashi et al., 2008)	ST-MC, MC TMS 11–2	2.3 · 10	23.8 % H <sub>2</sub> O, 1.2 % NaCl, 75 % glycerol	33.9	3.0 wt% TGCR(7) in decane	23,548
(Kobayashi et al., 2009)	AST-MC, MC arrays, WMS 1–1	10 · 150	H <sub>2</sub> O, 0.86 mol L – 1 NaCl	1	Decane, 3 wt% TGCR (7)	6,516
(Stolovicki et al., 2018)	Volcano Step (h = 6 $\mu\text{m}$ )	6 · 35	H <sub>2</sub> O	1	HFE 7500, 1 % FLo-surfactant	384
(Stolovicki et al., 2018)	Volcano Step (h = 12 $\mu\text{m}$ )	12 · 70	H <sub>2</sub> O	1	HFE 7500, 1 % FLo-surfactant	192
(Stolovicki et al., 2018)	Volcano Step (h = 20 $\mu\text{m}$ )	20 · 100	H <sub>2</sub> O	1	HFE 7500, 1 % FLo-surfactant	160
(Amstad et al., 2016)	Millipede (h = 20 $\mu\text{m}$ )	20 · 130	H <sub>2</sub> O, 10 wt% PEG (8)	8	FL oil, 1 wt% FLo-surfactant	550
(Amstad et al., 2016)	Millipede if upscaled (h = 20 $\mu\text{m}$ )	20 · 130	H <sub>2</sub> O, 10 wt% PEG (8)	8	FL oil, 1 wt% FLo-surfactant	550



**Table 4**

Overview of the productivities of upscaled spontaneous microfluidic emulsification devices reported in literature that produce droplets of < 80  $\mu\text{m}$ . The main focus was on oil-in-water emulsions, but the bottom seven rows are about water-in-oil emulsion generation devices. Information on the devices and components used can be found in Table 3. \*Indicates theoretical productivity when corrected for the dispersed phase viscosity (to 50 mPa s). The letter 'T' in the 'Effective area' or 'Productivity' column indicates a truly upscaled device with multiple rows of DFUs stacked; the letter 'S' indicates that a speculative effective area of 5 % was used by us; the letter 'P' that a speculative effective area was mentioned in that publication itself.

Article	Active DFUs (%)	Frequency per DFU ( $\text{s}^{-1}$ )	Productivity ( $\text{mL} / \text{h}$ )	Droplet size ( $\mu\text{m}$ )	CV (%)	Effective area	Productivity ( $\text{L}/(\text{m}^2 \text{h})$ )	Productivity* ( $\text{mL} / \text{h}$ )	Productivity* ( $\text{L}/(\text{m}^2 \text{h})$ )
This paper	100 %	19	0.057	5.2	2.7 %	5.0 % S	51 S	0.073	66 S
This paper	100 %	344	0.30	3.5	3.2 %	5.0 % S	271 S	0.38	345 S
This paper	100 %	7.8	0.21	12	7.8 %	5.0 % S	65 S	0.27	83 S
This paper	100 %	89	0.54	7.4	3.2 %	5.0 % S	167 S	0.69	214 S
This paper	100 %	6.9	3.4	32	3.8 %	–	–	4.3	–
This paper	100 %	8.3	4.0	32	2.8 %	–	–	5.0	–
(Van Dijke, Schroën, et al., 2010)	100 %	150	0.021	7.2	12.1 %	5.0 % S	9 S	0.021	9 S
(Van Dijke, Schroën, et al., 2010)	100 %	2,200	0.34	7.5	11.8 %	5.0 % S	146 S	0.023	10 S
(Sahin & Schroën, 2015)	100 %	1,061	0.053	9.3	4.0 %	4.4 % P	6,000 P	0.004	408P
(Sahin & Schroën, 2015)	100 %	136	0.19	28	4.5 %	4.4 % P	25,000 P	0.013	1,700P
Ten Klooster et al (2022)	93 %	58	10	11	10 %	5.0 % T	313 T	0.69	21 T
(Ofner et al., 2017)	100 %	70	26	81	2.8 %	5.0 % S	1,753 S	1.7	119 S
(Kobayashi et al., 2003)	missing	missing	3	39.1	< 3 %	1.0 % T	30 T	–	30 T
(Kobayashi et al., 2003)	missing	missing	6	38.6	< 3 %	1.0 % T	60 T	–	60 T
(Kobayashi et al., 2005b)	missing	50	–	40.9	1.3 %	5.2 % T	–	–	–
(Kobayashi et al., 2005b)	missing	10	–	34.9	1.9 %	5.2 % T	–	–	–
(Kobayashi et al., 2007)	100 %	14.5	0.0001	1.4	16.7 %	5.0 % S	4 S	0.00011	4 S
(Kobayashi et al., 2007)	100 %	missing	–	2.6	9.7 %	5.0 % S	–	–	–
(Kobayashi et al., 2007)	100 %	6.5	0.0008	3.5	8.5 %	5.0 % S	6 S	0.00079	6 S
(Kobayashi et al., 2001)	50 %	3	0.0005	5.2	2.0 %	5.0 % S	1 S	0.00048	1 S
(Kobayashi et al., 2005c)	60 %	3.3	23	31	10 %	4.1 % T	25 T	24	25 T
(Kobayashi et al., 2005c)	60 %	8.5	60	31	10 %	4.1 % T	66 T	58	63 T
(Kobayashi et al., 2010)	100 %	43	1.5	12	5.0 %	5.0 % S	80 S	1.5	80 S
(Vladisavljević et al., 2011)	97 %	14	12	27	(span 0.3)	11.7 % T	120 T	12	120 T
(Vladisavljević et al., 2011)	90 %	50	60	31.2	(span 0.25)	11.7 % T	600 T	24	240 T
(Vladisavljević et al., 2011)	50 %	250	248	35.6	(span 0.3)	11.7 % T	2,700 T	13	146 T
(Kobayashi et al., 2012)	100 %	40	1,230	87	2.0 %	10.4 % T	2,800 T	66	151 T
(Vladisavljević et al., 2018)	92 %	2.8	0.045	26	1.6 %	5.0 % S	46 S	0.0004	0.37 S
(Vladisavljević et al., 2018)	34 %	1.5	0.0051	14	4.6 %	5.0 % S	4 S	0.00004	0.034 S
(Kobayashi et al., 2008)	missing	missing	0.05	6.7	3.9 %	2.4 % T	2.22 T	0.05	2.2 T
(Kobayashi et al., 2008)	missing	1.1	–	7.1	2.8 %	2.4 % T	–	–	–
(Kobayashi et al., 2009)	40 %	200	87	45	2.5 %	9.8 % T	1,200 T	1.7	24 T
(Stolovicki et al., 2018)	100 %	1,500	29	30	5.2 %	5.0 % S	18,176 S	0.59	364 S
(Stolovicki et al., 2018)	100 %	1,063	51	51	4.8 %	5.0 % S	15,821 S	1.0	316 S
(Stolovicki et al., 2018)	100 %	341	91	96	2.6 %	5.0 % S	14,217 S	1.8	284 S
(Amstad et al., 2016)	100 %	188	100	75	3 %	0.6 % T	600 T	16.0	96 T

(continued on next page)



Table 4 (continued)

Article	Active DFUs (%)	Frequency per DFU (s <sup>-1</sup> )	Productivity (mL / h)	Droplet size (μm)	CV (%)	Effective area	Productivity (L/(m <sup>2</sup> h))	Productivity* (mL / h)	Productivity* (L/(m <sup>2</sup> h))
(Amstad et al., 2016)	100 %	188	100	75	3 %	11 % P	11,000 P	16.0	1,760P

Table A1

The calculated correction factors for the analysis of droplet sizes by the Matlab script, with their standard deviations, for the small, intermediate and large droplets produced with 2 wt% Tween 20 or 5 wt% WPI.

	Small	Intermediate	Large
Tween 20	0.906 ± 0.021	0.949 ± 0.012	0.911 ± 0.00024
WPI	0.883 ± 0.0042	0.922 ± 0.019	0.951 ± 0.0039

UPE<sub>10x2</sub> were almost twice as large as the droplets produced with UPE<sub>5x1</sub>, for both emulsifiers used (Figs. 3 and 4), which is in line with literature (Kobayashi, Mukataka, & Nakajima, 2004; Sugiura, Nakajima, Kumazawa, Iwamoto, & Seki, 2002; van Dijke, de Ruiter, et al., 2010).

Since we were interested in producing several emulsions with droplets of distinct sizes, we used the UPE<sub>10x2</sub> chip in the second pressure regime to produce larger monodisperse droplets, using 5 wt% WPI or 2 wt% Tween 20 (Figs. 3 & 4 respectively). For the UPE<sub>5x1</sub> chip, a much higher pressure would be required (Equation (2)) to reach this stage, whereas the droplet sizes remains roughly 1.6–1.8 times the center-to-center distance between two DFUs (Ten Klooster et al., 2019), which is similar for UPE<sub>5x1</sub> and UPE<sub>10x2</sub>. Overall, these larger droplet sizes are independent of emulsifier used (Figs. 3 & 4) and, as shown previously, of continuous and dispersed phase viscosities (Ten Klooster et al., 2019).

### 3.2. Droplet formation mechanism

During small droplet formation with UPE, two stages can be distinguished: the down time (filling) and necking time (Deng et al., 2021; Ten Klooster, van den Berg, Berton-Carabin, de Ruiter, & Schroën, 2022). During the down time, the DFU (re)fills if the applied pressure is higher than the Laplace pressure of the meniscus in the DFU, and this stage finishes when the dispersed phase leaps into the deeper continuous phase channel. This is also the starting point for necking, which finishes when the liquid thread, connecting the droplet to the oil in the DFU, breaks due to the interfacial tension force that overcomes the viscous

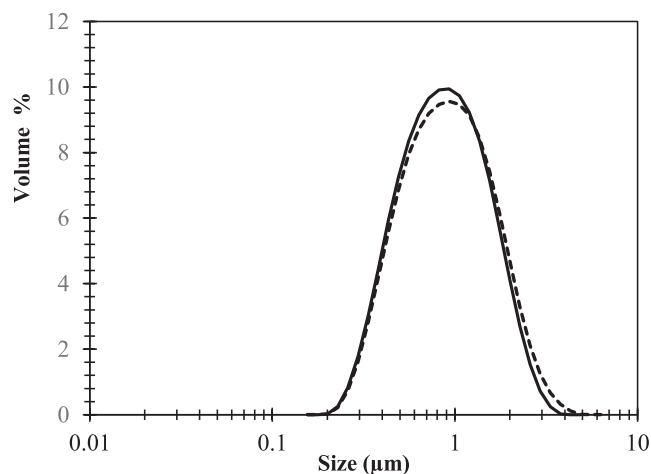


Fig. A1. Droplet size distributions of sonication-based broken-up small (dashed line) and large droplets (solid line) prepared with 2 wt% Tween 20.

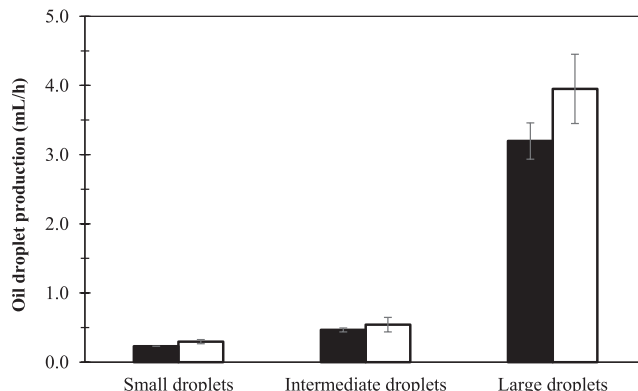


Fig. A2. The production of oil droplet as measured by image analysis (open bars) (section 2.7.1) and by collecting the emulsion and measuring its oil content (filled bars) (section 2.7.2) when using 5 wt% WPI in the continuous phase.

(and inertial) forces (Deng et al., 2021; Sugiura, Nakajima, Iwamoto, & Seki, 2001; Ten Klooster et al., 2022).

#### 3.2.1. Effect of emulsifier on droplet formation

For both UPE<sub>5x1</sub> and UPE<sub>10x2</sub>, a 3.5-fold higher pressure could be applied in the first pressure regime when comparing WPI with Tween 20 (Table 2). Possibly, the interfacial tension at the moment of droplet formation is higher for WPI because of its higher equilibrium interfacial tension (Bos & Van Vliet, 2001; Deng, Schroën, & de Ruiter, 2022; Muijlwijk, Hinderink, Ershov, Berton-Carabin, & Schroën, 2016). An additional explanation could be that WPI changes the contact angle that promotes wetting by the continuous phase upon irreversible protein adsorption at the glass surface, which therewith may increase the pressure stability of the system (Sahin et al., 2016).

As expected, the value of the blow-up pressure affects the productivity: when switching from 2 wt% Tween 20 to 5 wt% WPI, for UPE<sub>5x1</sub> a 5.2-fold higher production was found; for UPE<sub>10x2</sub> this was 2.5-fold higher; whereas in literature, a 2-fold lower productivity was found (Sahin et al., 2016). The difference in these values is most probably the results of differences in device design, and the components used. In the device used by Sahin et al., the Laplace pressure of the bare oil–water interface of the meniscus (~300 mbar, Equation (6)) was higher than the maximum pressure that could be applied for both emulsifiers (for Tween 20, 120 mbar and for WPI, 220 mbar) without blow-up occurring. As a result, emulsifiers have to adsorb before the DFU can refill, which is slower when using WPI than when using Tween 20 (Bos & Van Vliet, 2001; Deng et al., 2022; Muijlwijk et al., 2016), leading to lower productivity for their device (Sahin et al., 2016).

#### 3.2.2. Effect of dispersed phase supply channels on droplet formation

The blow-up pressure ( $\Delta P$ , Table 2) is about a 3.5- to 4-fold higher for UPE<sub>5x1</sub> compared to UPE<sub>10x2</sub> for both WPI and Tween 20. The blow-up pressure can be deduced as follows: the interfacial tension force during the necking stage can be assumed independent of the chip used. This implies that the maximum viscous force is equal for the chips, which results in an equal flow velocity at blow-up pressure (Stolovicki et al., 2018). This occurs when the necking volumetric flow rate of UPE<sub>5x1</sub> is a

fourfold lower than that of UPE<sub>10x2</sub> because the DFU area in UPE<sub>5x1</sub> is four times smaller. The flow resistance of the UPE<sub>5x1</sub> chip is around a 12.8-fold higher than that of the UPE<sub>10x2</sub> chip (Equation (2), 3, 4), which implies that the applied pressure has to be a 12.8-fold higher to obtain the same volumetric flow rate (Equation (5)). The resulting theoretical difference of a 3.2-fold (12.8/4) higher blow-up pressure for the UPE<sub>5x1</sub> chip compared to the UPE<sub>10x2</sub> chip is close to the experimental values (3.5-fold for Tween 20 and 4.1-fold for WPI, Table 2). This shows that the blow-up pressure can be estimated based on the dimensions of the DFU and dispersed phase supply channels, and that gives a clear handle for productivity enhancement.

### 3.3. Maximum productivities compared to literature

High productivities reported for microfluidic emulsification devices can be encountered in literature; for example 1.5 L/h (Gelin et al., 2020). These productivities are highly subjective to the droplet size and ingredients used. To put the results into perspective, Gelin and co-workers made hexane droplets of 45  $\mu\text{m}$ , with a viscosity that is a two hundredfold (60/0.3) lower than our rapeseed oil. Since productivity scales linearly with viscosity (and in a more complex way with droplet size), it is clear that comparing based on throughput only does not do full justice to the capacity of a system. In the next sections, we discuss how devices presented in literature could be compared and focus on spontaneous devices for their upscaling potential (section 1) (Schroën et al., 2015).

#### 3.3.1. The maximum true throughput

The maximum ‘true’ oil throughput of a device producing an O/W emulsion, in mL/h, can be a way to compare upscaled devices, for example when the goal is to produce monodisperse emulsion samples (Khalid et al., 2015; Krebs et al., 2012). Especially our 0.30 mL per h for 3.5- $\mu\text{m}$  (CV 3.2 %) rapeseed oil droplets, for 5 wt% WPI, is high compared to literature (Tables 3 and 4). The throughput for 7.4- $\mu\text{m}$  (CV 3.2 %) rapeseed oil droplets, using the UPE<sub>10x2</sub> chip with 5 wt% WPI, of 0.54 mL oil per h is high when compared to literature for droplets < 10  $\mu\text{m}$  and comparable to the study by Kobayashi et al., who produced 1.5 mL/h of 12- $\mu\text{m}$  (CV 5 %) rapeseed oil droplets (Kobayashi, Wada, Uemura, & Nakajima, 2010), when keeping in mind the larger droplets there. The high throughputs in the current research are also a result of the 100 % DFU activation that we achieved, which makes UPE devices stand out from others (Table 4).

The true oil throughput of larger droplets (32  $\mu\text{m}$ ) in the second pressure regime of  $\pm 4$  mL/h is high, especially since it was achieved with ‘only’ 8000 DFUs, showing the potential of this regime for producing larger monodisperse droplets (CVs of 3–4 %), although it might be difficult to further upscale this because the droplets need to interact for their formation. Higher true productivities for similar sized droplets have been reported by Kobayashi et al. (23 mL/h of 31- $\mu\text{m}$  rapeseed oil droplets with 211,000 DFUs) (Kobayashi et al., 2005c) and by Vladisavljević et al. (12 mL/h of 27- $\mu\text{m}$  rapeseed oil droplets with 23,000 DFUs) (Vladisavljević et al., 2011) (Table 4). The productivity per DFU for these  $\sim 30$ - $\mu\text{m}$  droplets is similar for these devices, including our UPE (Table 4).

#### 3.3.2. Surface area related productivity

Oil droplet productivity of microfluidic emulsification devices is often reported in terms of L/m<sup>2</sup>h (Table 3 & 4). This area-productivity can only be determined if devices in one way or another can be stacked (indicated with the letter ‘T’ in Table 4). An impressive area-productivity has been reported by Vladisavljević and coworkers of 120 L/m<sup>2</sup>h for the production of 27- $\mu\text{m}$  rapeseed oil droplets (Table 4) (Vladisavljević et al., 2011), and the microfluidic emulsification device called Multi EDGE showed a productivity of 300 L/m<sup>2</sup>h for the production of 10- $\mu\text{m}$  hexadecane droplets (ten Klooster et al., 2022). When correcting for the lower viscosity of hexadecane (3.4- versus 50 mPa s

for rapeseed oil (van Dijke, Kobayashi, et al., 2010)), denoted as (Productivity\*), this would result in 20 L/m<sup>2</sup>h for the production of smaller droplets.

It can be useful to calculate a theoretical area-productivity to envision what level of upscaling would be required to reach a specific product flow. For some devices reported in literature, such a theoretical area-productivity has been calculated (Amstad et al., 2016; Sahin & Schroën, 2015), which are indicated in Table 4 by the letter ‘P’. For the UPE devices presented here and other single-layer upscaled devices reported in literature, we calculated the area-productivity using the effective area of Multi EDGE (5 % (ten Klooster et al., 2022)) (Table 4, letter ‘S’) and corrected for the dispersed phase viscosity (productivity\*). We compare the productivity for each droplet size based on the actual size in the summary of Table 4. The value of 350 L/m<sup>2</sup>h for UPE<sub>5x1</sub> when operated with 5 wt% WPI leading to 3.5- $\mu\text{m}$  droplets compares favorably to the other devices that make small droplets.

### 3.4. Design insights upscaled microfluidic emulsification

The droplet size scales with three to four times the DFU height for constant height/width ratio of the device as shown in section 3.1.1 and in literature (Kobayashi, Mukataka, & Nakajima, 2005b; Kobayashi et al., 2007; Montessori, Lauricella, Stolovicki, Weitz, & Succi, 2019). The droplet size can be decreased by decreasing the DFU width (Kobayashi et al., 2007; Montessori et al., 2019; Ten Klooster et al., 2019), increasing the dispersed phase viscosity, or decreasing the continuous phase viscosity (Ten Klooster et al., 2019; van Dijke, de Ruiter, et al., 2010; van Dijke, Kobayashi, et al., 2010). A minimum DFU height-to-width ratio of  $\sim 2.5$  is required for monodisperse droplet formation (Kobayashi et al., 2004; Montessori et al., 2019).

Targeting small droplets will be at the expense of productivity per DFU. For example, decreasing the DFU dimensions by a factor of two, will decrease the maximum oil flow during necking by a factor of four (section 3.2.2), thus requiring four times as many DFUs for the same productivity. Since its surface area will be four times smaller, the same total pore area will still lead to the same productivity. So, depending on the practical limitations for the spacing between pores, this might influence the area-productivity. By reducing the smallest dimensions by a factor of two, the Laplace pressure increases by a factor of two (Equation (6)), which is important when targeting a device with a higher blow-up pressure than the Laplace pressure of the bare oil–water meniscus (see section 3.2.1 and below for the relevance of this). Please note that if the dimensions of all channels are decreased by a factor of two, the flow resistance, and thereby the blow-up pressure, increases by a factor of 16 (Equation (2)), which may negatively affect the energy efficiency of the device.

Not only the DFU design, but also the sub-structure design leading to the DFUs will influence the overall productivity and pressure stability. When the blow-up pressure is higher than the Laplace pressure of a bare oil–water interface (Equation (6)) (section 3.2 & 3.2.1) (Ten Klooster et al., 2022), productivity can be greatly enhanced, which also holds for some of our UPE-devices as stated earlier (Table 2). By designing the device in such a way, no surfactant adsorption is required for refilling of the DFU to take place, and thus down time is reduced (section 3.2 & 3.2.1). For example, the productivity of UPE<sub>10x2</sub> can be improved by increasing its blow-up pressure through increasing the flow resistance of the main dispersed phase supply channels (plateaus, Fig. 1) (Table 2, Equation (2), (3), (4), (5)). Please be aware that the blow-up pressure is highly dependent on the type of oil, continuous phase, emulsifier, and on the dimensions of the DFU itself (Sahin et al., 2016; Ten Klooster et al., 2019). A high blow-up pressure by a high flow resistance of sub-structures will also have advantages for DFU activation and, above all, for process stability (ten Klooster et al., 2022). Yet, the blow-up pressure should not be too high to remain energy-efficient. In this way, the productivity of many devices reported in literature (Kobayashi, Nakajima, & Mukataka, 2003; Kobayashi et al., 2008, 2007; ten Klooster et al.,

2022; Vladislavjević et al., 2018) may be improved by increasing substructure resistance as far as technical advances allow (ten Klooster et al., 2022).

When the dispersed phase flow rate is known, the device can be operated to make a specific oil volume fraction by applying a specific continuous phase flow rate. The required pressure follows from Equations (2) & (5). If the width and height of the channels are too large, this can hinder regulating the continuous phase flow rate and the gradual fill of droplets into this channel. If they are too small, a significant pressure drop causes distal DFUs to operate close to blow-up, whereas the upstream DFUs run below their maximum production rate. For UPE<sub>10x2</sub> when using Tween 20 (Table 2), the pressure over the continuous phase (60 mbar) was in the range of the pressure applied over the dispersed phase (260 mbar), which may explain the higher CV (7.8 %) compared to the other emulsions produced (often 3 %) (Figs. 3 and 4).

Away from the droplet size that was discussed earlier, the ingredients used to produce emulsions with such microfluidic chips have a major influence on the productivity. The viscosity of the oil scales inversely with the productivity (Kobayashi, Mukataka, & Nakajima, 2005a; van Dijke, Kobayashi, et al., 2010), and the interfacial tension between water and oil scales directly with the productivity (Kobayashi et al., 2005c, 2005a). Furthermore, productivity decreases with increasing continuous phase viscosity (Kobayashi et al., 2009; van Dijke, Kobayashi, et al., 2010). The type and concentration of emulsifier do affect the productivity as well, and its effect can even be dependent on the chip design (Section 3.2.1). Generally, the productivity increases with higher (dynamic) interfacial tension (Kobayashi et al., 2005c, 2005a) and with improved device wetting by the continuous phase (Sahin et al., 2016). However, this is not that well-understood yet to allow for a prediction of the productivity based on the emulsifier and its characteristic behavior both at the oil–water interface and at the surface of the microchip walls.

#### 4. Conclusion

We showed that the Upscaled Partitioned EDGE emulsification device (UPE) can produce highly monodisperse rapeseed oil droplets using Tween 20 and whey proteins as prominent representatives of food-grade surfactant and protein emulsifiers, respectively. Productivities were 0.3 mL/h for 3.5- $\mu$ m droplets (CV 3.2 %) with 11,000 DFUs of 5x1  $\mu$ m; 0.5 mL/h for 7- $\mu$ m droplets (CV 3.2 %) with 8,000 DFUs of 10x2  $\mu$ m; and with the same chip operated at higher pressures, 4 mL/h for 32- $\mu$ m droplets (CV 3–4 %). These productivities are high compared to other devices presented in literature.

Further optimization of the chips is possible: the relatively small continuous phase channel dimensions generated a pressure drop over the continuous phase that negatively influences monodisperse droplet productivity, which resulted in a CV of 7 % for Tween 20 (instead of 3 %). We also show that the pressure at which the DFUs produced larger droplets can be deduced by calculating the flow velocity based on the Hagen-Poiseuille equation. This pressure should be higher than the Laplace pressure of the meniscus inside the DFU without any surfactant adsorbed to generate a fast refill of the DFU. The choice of ingredients influences the emulsion production as well: the productivity is higher when using WPI than when using Tween 20, which could be a result of the higher (dynamic) interfacial tension and/or improved channel wetting by the continuous phase.

The above productivities and design insights will bring us closer to food emulsions products produced with microfluidics. Current productivities are already sufficient to address knotty problems in food research that we are currently working on, such as the effect of droplet size on chemical and physical stability of emulsions, which was only possible because of these upscaling efforts.

#### Funding source

This research was funded by the Dutch Research Council (NWO),

Grant No 731.017.301.

#### CRedit authorship contribution statement

**Sten ten Klooster:** Conceptualization, Data curation, Formal analysis, Investigation, Methodology, Visualization, Writing – original draft. **Claire Berton-Carabin:** Conceptualization, Investigation, Methodology, Writing – review & editing, Supervision. **Karin Schroën:** Investigation, Methodology, Writing – review & editing, Supervision, Funding acquisition.

#### Declaration of Competing Interest

The authors declare that they have no known competing financial interests or personal relationships that could have appeared to influence the work reported in this paper.

#### Acknowledgements

We thank our technician Maurice Strubel for his excellent technical assistance regarding the equipment used within this research, we thank Justin Tauber for writing the Matlab script, and we thank Jolet de Ruiter for her Matlab assistance and for her assistance regarding the UPE chip design.

#### Appendix

#### References

- Amstad, E., Chemama, M., Eggersdorfer, M., Arriaga, L. R., Brenner, M. P., & Weitz, D. A. (2016). Robust scalable high throughput production of monodisperse drops. *Lab on a Chip*, 16(21), 4163–4172.
- Berton, C., Genot, C., & Ropers, M.-H. (2011). Quantification of unadsorbed protein and surfactant emulsifiers in oil-in-water emulsions. *Journal of Colloid and Interface Science*, 354(2), 739–748. <https://doi.org/10.1016/j.jcis.2010.11.055>
- Bos, M. A., & Van Vliet, T. (2001). Interfacial rheological properties of adsorbed protein layers and surfactants: A review. *Advances in Colloid and Interface Science*, 91(3), 437–471.
- Deng, B., Schroën, K., & de Ruiter, J. (2021). Effects of dynamic adsorption on bubble formation and coalescence in partitioned-EDGE devices. *Journal of Colloid and Interface Science*, 602, 316–324.
- Deng, B., Schroën, K., & de Ruiter, J. (2022). Dynamics of bubble formation in spontaneous microfluidic devices: Controlling dynamic adsorption via liquid phase properties. *Journal of Colloid and Interface Science*, 622, 218–227.
- Gijsbertsen-Abrahamse, A. J., van der Padt, A., & Boom, R. M. (2004). Status of cross-flow membrane emulsification and outlook for industrial application. *Journal of Membrane Science*, 230(1), 149–159. <https://doi.org/10.1016/j.memsci.2003.11.006>
- Hinderink, E. B. A., de Ruiter, J., de Leeuw, J., Schroën, K., Sagis, L. M. C., & Berton-Carabin, C. C. (2021). Early film formation in protein-stabilised emulsions: Insights from a microfluidic approach. *Food Hydrocolloids*, 118, Article 106785.
- Jacobs, N. J., & Vandenmark, P. J. (1960). Colorimetric method for determination of triglycerides. *Arch Biochem. Biophys*, 88, 250–255.
- Kawakatsu, T., Kikuchi, Y., & Nakajima, M. (1997). Regular-sized cell creation in microchannel emulsification by visual microprocessing method. *Journal of the American Oil Chemists' Society*, 74(3), 317–321.
- Khalid, N., Kobayashi, I., Wang, Z., Neves, M. A., Uemura, K., Nakajima, M., & Nabetani, H. (2015). Formulation of monodisperse oil-in-water emulsions loaded with ergocalciferol and cholecalciferol by microchannel emulsification: Insights of production characteristics and stability. *International Journal of Food Science & Technology*, 50(8), 1807–1814.
- Kobayashi, I., Mukataka, S., & Nakajima, M. (2004). CFD simulation and analysis of emulsion droplet formation from straight-through microchannels. *Langmuir*, 20(22), 9868–9877.
- Kobayashi, I., Mukataka, S., & Nakajima, M. (2005a). Effects of type and physical properties of oil phase on oil-in-water emulsion droplet formation in straight-through microchannel emulsification, experimental and CFD studies. *Langmuir*, 21(13), 5722–5730.
- Kobayashi, I., Mukataka, S., & Nakajima, M. (2005b). Novel asymmetric through-hole array microfabricated on a silicon plate for formulating monodisperse emulsions. *Langmuir: The ACS Journal of Surfaces and Colloids*, 21(17), 7629–7632. <https://doi.org/10.1021/la050915x>
- Kobayashi, I., Mukataka, S., & Nakajima, M. (2005c). Production of monodisperse oil-in-water emulsions using a large silicon straight-through microchannel plate. *Industrial & Engineering Chemistry Research*, 44(15), 5852–5856.

- Kobayashi, I., Murayama, Y., Kuroiwa, T., Uemura, K., & Nakajima, M. (2009). Production of monodisperse water-in-oil emulsions consisting of highly uniform droplets using asymmetric straight-through microchannel arrays. *Microfluidics and Nanofluidics*, 7(1), 107.
- Kobayashi, I., Nakajima, M., & Mukataka, S. (2003). Preparation characteristics of oil-in-water emulsions using differently charged surfactants in straight-through microchannel emulsification. *Colloids and Surfaces A: Physicochemical and Engineering Aspects*, 229(1–3), 33–41.
- Kobayashi, I., Nakajima, M., Nabetani, H., Kikuchi, Y., Shohno, A., & Satoh, K. (2001). Preparation of micron-scale monodisperse oil-in-water microspheres by microchannel emulsification. *Journal of the American Oil Chemists' Society*, 78(8), 797–802.
- Kobayashi, I., Neves, M. A., Wada, Y., Uemura, K., & Nakajima, M. (2012). Large microchannel emulsification device for mass producing uniformly sized droplets on a liter per hour scale. *Green Processing and Synthesis*, 1(4), 353–362.
- Kobayashi, I., Takano, T., Maeda, R., Wada, Y., Uemura, K., & Nakajima, M. (2008). Straight-through microchannel devices for generating monodisperse emulsion droplets several microns in size. *Microfluidics and Nanofluidics*, 4(3), 167–177.
- Kobayashi, I., Uemura, K., & Nakajima, M. (2007). Formulation of monodisperse emulsions using submicron-channel arrays. *Colloids and Surfaces A: Physicochemical and Engineering Aspects*, 296(1–3), 285–289.
- Kobayashi, I., Wada, Y., Uemura, K., & Nakajima, M. (2010). Microchannel emulsification for mass production of uniform fine droplets: Integration of microchannel arrays on a chip. *Microfluidics and Nanofluidics*, 8(2), 255–262.
- Krebs, T., Schroën, K., & Boom, R. (2012). Coalescence dynamics of surfactant-stabilized emulsions studied with microfluidics. *Soft Matter*, 8(41), 10650–10657.
- Leal-Calderon, F., Schmitt, V., & Bibette, J. (2007). *Emulsion science: Basic principles*. Springer Science & Business Media.
- Montessori, A., Lauricella, M., Stolovicki, E., Weitz, D. A., & Succi, S. (2019). Jetting to dripping transition: Critical aspect ratio in step emulsifiers. *Physics of Fluids*, 31(2), 21703.
- Muijlwijk, K., Colijn, I., Harsono, H., Krebs, T., Berton-Carabin, C., & Schroën, K. (2017). Coalescence of protein-stabilised emulsions studied with microfluidics. *Food Hydrocolloids*, 70, 96–104.
- Muijlwijk, K., Hinderink, E., Ershov, D., Berton-Carabin, C., & Schroën, K. (2016). Interfacial tension measured at high expansion rates and within milliseconds using microfluidics. *Journal of Colloid and Interface Science*, 470, 71–79.
- Neves, M. A., Wang, Z., Kobayashi, I., & Nakajima, M. (2017). Assessment of oxidative stability in fish oil-in-water emulsions: Effect of emulsification process, droplet size and storage temperature. *Journal of Food Process Engineering*, 40(1), e12316.
- Ofner, A., Moore, D. G., Rühls, P. A., Schwendimann, P., Eggersdorfer, M., Amstad, E., ... Studart, A. R. (2017). High-throughput step emulsification for the production of functional materials using a glass microfluidic device. *Macromolecular Chemistry and Physics*, 218(2).
- Sahin, S., Bliznyuk, O., Cordova, A. R., & Schroën, K. (2016). Microfluidic EDGE emulsification: The importance of interface interactions on droplet formation and pressure stability. *Scientific Reports*, 6, 26407.
- Sahin, S., & Schroën, K. (2015). Partitioned EDGE devices for high throughput production of monodisperse emulsion droplets with two distinct sizes. *Lab on a Chip*, 15(11), 2486–2495.
- Schroën, K., Berton-Carabin, C., Renard, D., Marquis, M., Boire, A., Cochereau, R., ... Marze, S. (2021). Droplet microfluidics for food and nutrition applications. *Micromachines*, 12(8), 863.
- Schroën, K., Bliznyuk, O., Muijlwijk, K., Sahin, S., & Berton-Carabin, C. C. (2015). Microfluidic emulsification devices: From micrometer insights to large-scale food emulsion production. *Current Opinion in Food Science*, 3, 33–40.
- Schroën, K., Bliznyuk, O., Muijlwijk, K., Sahin, S., & Berton-Carabin, C. C. (2015). Microfluidic emulsification devices: From micrometer insights to large-scale food emulsion production. *Current Opinion in Food Science*, 3, 33–40.
- Shang, L., Cheng, Y., & Zhao, Y. (2017). Emerging droplet microfluidics. *Chemical Reviews*, 117(12), 7964–8040.
- Stolovicki, E., Ziblat, R., & Weitz, D. A. (2018). Throughput enhancement of parallel step emulsifier devices by shear-free and efficient nozzle clearance. *Lab on a Chip*, 18(1), 132–138.
- Sugiura, S., Nakajima, M., Iwamoto, S., & Seki, M. (2001). Interfacial tension driven monodispersed droplet formation from microfabricated channel array. *Langmuir*, 17(18), 5562–5566.
- Sugiura, S., Nakajima, M., Kumazawa, N., Iwamoto, S., & Seki, M. (2002). Characterization of spontaneous transformation-based droplet formation during microchannel emulsification. *The Journal of Physical Chemistry B*, 106(36), 9405–9409. <https://doi.org/10.1021/jp0259871>
- Teh, S.-Y., Lin, R., Hung, L.-H., & Lee, A. P. (2008). Droplet microfluidics. *Lab on a Chip*, 8(2), 198–220.
- Ten Klooster, S., van den Berg, J., Berton-Carabin, C., de Ruiter, J., & Schroën, K. (2022). Upscaling microfluidic emulsification: The importance of sub-structure design in EDGE devices. *Chemical Engineering Science*, 117993. <https://doi.org/10.1016/j.CES.2022.117993>
- Klooster, T., Sahin, S., & Schroën, K. (2019). Monodisperse droplet formation by spontaneous and interaction based mechanisms in partitioned EDGE microfluidic device. *Scientific Reports*, 9(1), 1–12. <https://doi.org/10.1038/s41598-019-44239-7>
- Trinder, P. (1969). Quantitative determination of triglyceride using GPO-PAP method. *Ann Biochem*, 6, 24–27.
- van Dijke, K. C., Schroën, K., van der Padt, A., & Boom, R. (2010). EDGE emulsification for food-grade dispersions. *Journal of Food Engineering*, 97(3), 348–354.
- van Dijke, K. C., Veldhuis, G., Schroën, K., & Boom, R. M. (2010). Simultaneous formation of many droplets in a single microfluidic droplet formation unit. *AIChE Journal*, 56(3), 833–836.
- van Dijke, K., de Ruiter, R., Schroën, K., & Boom, R. (2010). The mechanism of droplet formation in microfluidic EDGE systems. *Soft Matter*, 6(2), 321–330.
- van Dijke, K., Veldhuis, G., Schroën, K., & Boom, R. (2009). Parallelized edge-based droplet generation (EDGE) devices. *Lab on a Chip*, 9(19), 2824–2830.
- Dijke, V., Kobayashi, I., Schroën, K., Uemura, K., Nakajima, M., & Boom, R. (2010). Effect of viscosities of dispersed and continuous phases in microchannel oil-in-water emulsification. *Microfluidics and Nanofluidics*, 9(1), 77–85. <https://doi.org/10.1007/s10404-009-0521-7>
- Vladislavjević, G. T., Kobayashi, I., & Nakajima, M. (2012). Production of uniform droplets using membrane, microchannel and microfluidic emulsification devices. *Microfluidics and Nanofluidics*, 13(1), 151–178.
- Vladislavjević, G. T., Ekanem, E. E., Zhang, Z., Khalid, N., Kobayashi, I., & Nakajima, M. (2018). Long-term stability of droplet production by microchannel (step) emulsification in microfluidic silicon chips with large number of terraced microchannels. *Chemical Engineering Journal*, 333(Supplement C), 380–391. <https://doi.org/10.1016/j.cej.2017.09.141>
- Vladislavjević, G. T., Kobayashi, I., & Nakajima, M. (2011). Effect of dispersed phase viscosity on maximum droplet generation frequency in microchannel emulsification using asymmetric straight-through channels. *Microfluidics and Nanofluidics*, 10(6), 1199–1209.
- Zhang, Y., Kobayashi, I., Neves, M. A., Uemura, K., & Nakajima, M. (2015). Effects of surface treatment and storage conditions of silicon microchannel emulsification plates on their surface hydrophilicity and preparation of soybean oil-in-water emulsion droplets. *Journal of Food Engineering*, 167, 106–113.
- Zhu, P., & Wang, L. (2017). Passive and active droplet generation with microfluidics: A review. *Lab on a Chip*, 17(1), 34–75.